References and Notes

1. R. B. Hargraves and N. Petersen, *Icarus* **16**, 223 (1972).
2. R. B. Hargraves, D. W. Collinson, C. R. Spitzer, *Science* **194**, 84 (1976).
3. R. W. Shorthill, H. J. Moore, R. E. Hutton, R. F. Scott, C. R. Spitzer, *ibid.*, p. 1309.
4. S. L. Hess, R. M. Henry, C. B. Leovy, J. A. Ryan, J. E. Tillman, T. E. Chamberlain, H. L. Cole, R. G. Dutton, G. C. Greene, W. E. Simon, J. L. Mitchell, *ibid.* **194**, 78 (1976); S. L. Hess, personal communication.
5. T. Mutch, S. Grenander, K. Jones, W. Patterson, R. Arvidson, E. Guinness, P. Avrin, E. Carlston, A. Binder, C. Sagan, E. Dunham, P. Fox, D. Pieri, F. Huck, C. Rowland, G. Taylor, S. Wall, R. Kahn, E. Levinthal, S. Liebes, R. Tucker, E. Morris, J. Pollack, R. Saunders, M. Wolf, *Science* **194**, 1277 (1976).
6. F. O. Huck, H. F. McCall, W. R. Patterson, G. R. Taylor, *Space Sci. Instrum.* **1**, 189 (1975).
7. L. Kelly, F. O. Huck, R. E. Arvidson, NASA TN-X-72778 (1975).
8. S. Park and F. O. Huck, *Appl. Opt.*, in press.
9. Reflectance can be derived by normalizing the preamplifier voltage for each channel to the voltage obtained for each channel for one of the reference test chart patches mounted on the lander.

$$\frac{V_{i,m}}{V_{i,RTC}} = \frac{C_i \int_0^\infty \tau_i(\lambda)\rho(\lambda)_m\, \phi_m(i,e,g,\lambda)\,d\lambda}{C_i \int_0^\infty \tau_i(\lambda)\rho(\lambda)_{RTC}\, \phi_{RTC}(i,e,g,\lambda)\,d\lambda} \quad (1)$$

where $V_{i,m}$ is the preamplifier voltage for the ith channel imaging the magnetic material, $V_{i,RTC}$ is the equivalent for imaging one of the test patches, C_i is a channel-dependent calibration constant, and $\tau_i(\lambda)$ is the channel dependent transfer function, which is the product of the camera optical throughput, solar irradiance, atmospheric transmittance, and photosensor responsivity; $\rho(\lambda)_m$ is the normal albedo of the magnetic material, and $\phi_m(i,e,g,\lambda)$ is its photometric function, where i is the incidence angle, e is the emission angle, g is the phase angle, and λ is the wavelength. $\rho(\lambda)_{RTC}$ and $\phi_{RTC}(i,e,g,\lambda)$ are the corresponding functions for one of the test patches. Since the test patches have a Lambertian photometric function (*10*), and since the blue, green, red, and IR 1 channels can be approximated as single wavelength samples, this equation reduces to:

$$\rho(\lambda)_{i,m}\, \phi_{i,m}(i,e,g,\lambda) = \frac{V_{i,m}}{V_{i,RTC}}\rho(\lambda)_{RTC} \cos i \quad (2)$$

10. Gray patch reflectances of the RTC have been measured over a wide range of lighting and viewing geometry. The ratio of measured reflectance to that of an ideal Lambertian scatterer deviates from unity by no more than ± 10 percent. (A Lambertian surface scatters light equally in all directions.) In addition, the gray patch reflectances are not strongly wavelength dependent [see S. Wall, E. Burcher, D. Jobson, NASA TN-C-72762 (1975)]. Note that an additional error associated with radiometric calibration with the test patches is that they are located atop the lander and hence may receive reflected light from parts of the lander structure. This impairs the accuracy of absolute radiometric calibration since $\tau_i(\lambda)$ is then different for the numerator and denominator in Eq. 1 (*9*). Since the lander is painted with spectrally flat material, light reflected from the lander probably only serves to change the denominator by some constant. Problems do arise, however, in directly comparing the RTC and backhoe magnets since one is near the martian surface and one near the spacecraft. Analysis is underway to estimate the magnitude of lander-reflected light.
11. The backhoe image used was 11B040/040. For this image $i = 55°$, $e = 20°$, $g = 65°$. RTC magnet images were 12B032/034 and 12B069/039. RTC magnet reflectivities were nearly identical. For these images $i = 73°$, $e = 21°$, $g = 78°$. The trench image was 11A147/026, and $i = 60°$, $e = 25°$, $g = 65°$. Values for the trench lighting and viewing angles are only known to 20 percent because of uncertainties in the trench topography.
12. B. C. Clark, A. K. Baird, H. J. Rose, P. Toulmin, K. Keil, A. Castro, W. Kelliher, C. Rowe, P. Evans, *Science* **194**, 1284 (1976).
13. Sample provided by K. S. Deffeyes.
14. R. L. Huguenin, *J. Geophys. Res.* **78**, 8481 (1973).
15. W. A. Deer *et al.*, *Rock Forming Minerals*, (Wiley, New York, 1962), vol. 5.
16. J. T. O'Connor, *J. Geophys. Res.* **73**, 5301 (1968).
17. J. B. Adams and T. B. McCord, *ibid.* **74**, 4851 (1969).

18. Supported in part by the NASA Langley Research Center. We acknowledge with thanks the assistance of the Surface Sampler and Lander Imaging Teams in obtaining the pictures of the magnetic arrays on which our interpretations are based.

15 November 1976

The Environs of Viking 2 Lander

Abstract. *Forty-six days after Viking 1 landed, Viking 2 landed in Utopia Planitia, about 6500 kilometers away from the landing site of Viking 1. Images show that in the immediate vicinity of the Viking 2 landing site the surface is covered with rocks, some of which are partially buried, and fine-grained materials. The surface sampler, the lander cameras, engineering sensors, and some data from the other lander experiments were used to investigate the properties of the surface. Lander 2 has a more homogeneous surface, more coarse-grained material, an extensive crust, small rocks or clods which seem to be difficult to collect, and more extensive erosion by the retroengine exhaust gases than lander 1. A report on the physical properties of the martian surface based on data obtained through sol 58 on Viking 2 and a brief description of activities on Viking 1 after sol 36 are given.*

This report is primarily concerned with Viking 2 lander (VL2) data; however, some of the results obtained on Viking 1 after sol 36 will be reported. Earlier reports (*1, 2*) on the "soil" (*3*) properties of Mars were based on data obtained during the first 36 sols (*4*) of Viking 1 lander (VL1).

The dynamics of both landings were similar—an almost vertical descent during the last 10 seconds and a "soft" touchdown—but minor variations occurred. The activities of the surface sampler on VL2 were also similar to those carried out on VL1 with the addition that samples were obtained from under rocks for the biology and gas chromatograph–mass spectrometer (GCMS) experiments.

The surface materials in the sample field at Utopia Planitia can be described as blocks and fragments set in a matrix of finer-grained material (Figs. 1–3). Beyond the sample field, small dunes (pitted by rocks propelled by the engine exhausts) indicate a local wind direction near 320°. Blocks within the sample field attain dimensions of 0.65 by 0.23 m. Because of the viewing angles, the third dimension of blocks normally cannot be measured and much of the interblock surface is obscured. Finer-grained materials between rocks and fragments are present as fillets, small drifts, a weak platy crust, and subcrust materials; small clods and rock fragments are abundant everywhere between the rocks. Unlike the VL1 site at Chryse where the sample field could be divided into an area underlain by very fine-grained material and a rocky area (*1, 2*), Utopia Planitia is more uniform. The sample field at Utopia Planitia near footpad 3 and the ejected shroud are relatively rock-free, but materials there appear similar to those elsewhere (Fig. 2).

Deposits of cross-bedded drifts superposed on a rocky substrate, which covered extensive areas at the VL1 site, are virtually absent at Utopia Planitia. The rocky, deflated appearance of the VL2 site is consistent with orbital images of the site, in particular, and the region from 44°N to 48°N in general. Orbital images of the northern latitudes show partially stripped lava flows and ejecta blankets, hexagonal to reticulate structural patterns enhanced by erosion and deflation, secondary craters standing in stark relief because of deflation, and deflation hollows. These features are found in the general area of the VL2 landing site. There is no evidence for a thick aeolian mantle of fines or dune deposits as had been expected by many members of the landing site selection team.

Touchdown. Landing conditions for both VL1 and VL2 were close to nominal, with the exception of an anomaly which occurred during the last 0.4 second of the VL2 decent when there was a sudden reduction in the velocity at touchdown. Nominal conditions during the last 10 seconds before landing are vertical descent at a constant velocity of 2.44 m/sec and a horizontal attitude controlled by the lander radar and guidance system. The thrust of the descent engines is terminated upon contact of the footpads with the surface. The time interval between surface contact and the beginning of thrust decay is about 20 msec, and the decay time constant is about 30 msec. Touchdown parameters are given in Table 1.

The average leg stroke on VL1 was larger than on VL2. These data were at first surprising because both landers nominally appeared to have the same ki-

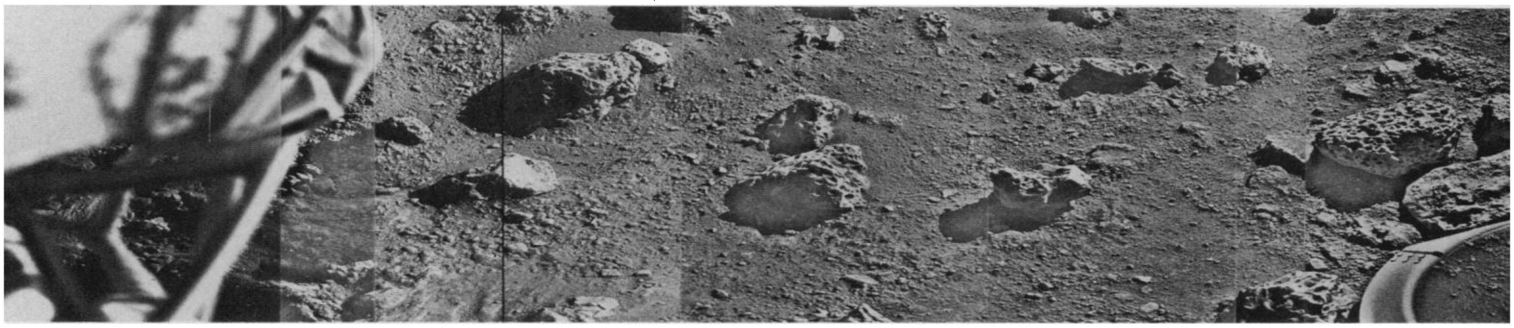

Fig. 1. Mosaic of the foreground from camera 2 on VL2. The surface sampler housing is to the far left, and footpad 3 is to the far right. Erosion from retro-engine 2 is evident (either side of the vertical black line). During the touchdown sequence, material was deposited in the footpad and the footpad impacted the rocks to the front.

netic energy at touchdown, yet a much larger fraction of this energy was removed by the energy absorbers in the primary struts on VL1 than on VL2. Leg 2 and leg 3 strokes determined from stroke gages and leg travel for VL2 are the same (footpad 1 is not in the field of view) and imply that the load limiters at the secondary strut attachment did not yield so that energy dissipation was essentially due to the crushing of the honeycomb tube-core cartridge of the primary struts. This result suggested that a larger fraction of the remaining energy must have been removed by the penetration of the VL2 footpads into the martian surface but a comparison of the footpad penetration of the two spacecraft indicates that the opposite is true.

One can resolve the problem by considering data on valve settings of the descent engines just prior to VL2 touchdown. During the last 0.43 second, the thrust levels of engines 1, 2, and 3 increased by about 14, 81, and 91 percent, respectively, because the terminal descent and landing radar system locked onto a false target. The impulse associated with the increase in the total thrust level is about 1360 newton-sec and produced an incremental velocity change of about 0.49 m/sec. The velocity of VL2 at surface contact is near 1.98 m/sec and less than the nominal descent value of 2.47 m/sec which prevailed before the thrust suddenly increased. This smaller velocity is compatible with the smaller leg strokes on VL2. Since the characteristics of the leg force–stroke are known, the energy absorbed by the primary strut in each leg is readily determined from the observed stroke. The energies absorbed by the stroking of the primary struts are 970 and 550 newton-m for VL1 and VL2, respectively, for the average stroke values listed in Table 1. Because the kinetic energies associated with the touchdown velocities (Table 1) are 1900 and 1170 newton-m for VL1 and VL2, respectively, the ratio of the energy absorbed by the primary strut stroking to the initial kinetic energy is 51 and 47 percent, respectively. From these corrected velocity and energy values one concludes that the energy ratios of both landers are roughly the same and that about half the kinetic energy present at touchdown was removed by primary strut stroking. More detailed energy balance calculations will be made at a later date.

Spacecraft tilt. Both landers are tilted more than indicated by the leg strokes, suggesting variations in the elevations of the local terrain. Leg stroking on VL1 rotates the plane of the spacecraft 1.9° to a plane through the bottom of the footpads. This tilt is along the same azimuth but smaller than the 3° tilt of the spacecraft with respect to the gravity vector measured with the guidance and control system and that determined from the horizon viewed by the cameras. This observation implies that the footpad plane is tilted 1.1° relative to the horizontal and the general surface defined by the horizon. Leg stroking on VL2 rotates the plane of the spacecraft 2.2° relative to the footpad plane. Tilt measured by the guidance and control system is 8.2° and much larger than 2.2°. Tilt with respect to the local horizon measured with the cameras is 8.3° along an azimuth of 280°. Thus, 6° of tilt must be accounted for by local conditions. One or more footpads must be resting in a depression or on a rock. The presence of rocks adjacent to footpad 3 (Figs. 1 and 2) and footpad 2 of VL2 suggests that the footpads themselves may be resting on rocks. Shallow linear depressions are also visible in the field of view so that it is entirely possible that footpad 1 of VL2 may be in a depression.

Table 1. Touchdown parameters for VL1 and VL2.

Parameter	VL1	VL2
Touchdown velocity (m/sec)	2.49	1.98
Latitude	22.46°N	47.97°N
Longitude	48.01°W	225.67°W
Leg 1 stroke, by stroke gauge (cm)	7.0	2.5 to 3.2
Leg 2 stroke, by stroke gauge (and footpad travel) (cm)	3.2 (2.8)	7.6 (7.6)
Leg 3 stroke, by stroke gauge (and footpad travel) (cm)	8.3 (8.3)	1.3 (1.3)
Footpad 1 penetration (cm)	No data	No data
Footpad 2 penetration (cm)	16.5	2.5
Footpad 3 penetration (cm)	3.6	0 to 0.3
Leg azimuth (east of north)	321.9°	209.1°
Tilt angle (relative to gravity vector)	3.0°	8.2°
Tilt azimuth (east of north)	285.2°	277.7°
Landed mass (kg)	613	600

Soil erosion. Figure 1 reveals evidence of soil erosion in the vicinity of engine 2 (left side, foreground). The erosion appears to be a scrubbing of the surface which removed a small layer of fines, exposing the coarser material below. These erosional results are similar to those that were obtained in Earth-based tests conducted under simulated martian conditions with a lunar nominal soil as the plume impingement surface. In the Earth-based tests only a surface scrubbing of fine material was observed on lunar nominal soil in either compacted or uncompacted density states. No test produced a crater below the engine deeper than 5 cm, and no test deposited a layer deeper than 8 mm or removed a layer deeper than 2 mm anywhere in the sample field area.

For a short time interval just prior to

thrust termination on VL2, the anomalous increase in thrust subjected the surface to almost a doubling of the plume impingement pressure and to the viscous shearing stresses exerted along the gas-surface interface. Thus, it is likely that a larger dust cloud resulted from VL2 than from VL1.

These higher surface disturbance stresses are also consistent with the larger erosional area near engine 2 on VL2 by comparison with VL1. (Compare, for example, the plan view shown in Fig. 2a with that in Fig. 2b.)

The rapid increase and subsequent shutdown transient on VL2 disturbed soil which subsequently landed inside of footpad 3. Material apparently was also deposited in the undeployed S band antenna dish. This phenomenon has been observed often in Earth-based tests during the shutdown transient. In such tests, soil has been observed to rise nearly vertically and follow a high arching trajectory. Such a disturbance in the case of VL2 was fortuitous because it provided information concerning particle size distribution down to the resolution of the camera system (about 0.7 mm due to the overlapping of image scans). Some of the results from the particle size distribution investigations are included later in this report.

Surface sampler activities. These activities for VL2 were similar to those for VL1 with important exceptions: (i) the period of intensive operations was longer for VL2 (through sol 58 for VL2 as compared with sol 41 for VL1); (ii) rocks were nudged and pushed, and samples were obtained from the newly exposed surfaces beneath the rocks; (iii) endeavors to collect coarse materials were not entirely successful for VL2; and (iv) small, thin, platy objects up to several centimeters in diameter were lifted to form a dome, dragged, and excavated by the surface sampler. Surface sampler activities related to the physical properties experiment for VL2 are summarized in Table 2.

After ejection of the protective shroud (*1*) on sol 1, a shadowed picture was taken beneath retro-engine 2, but small (centimeter size) linear depressions extended in a direction consistent with engine orientation relative to the local surface. Pictures repeated on VL2 sol 57 with better lighting will be analyzed later.

Rock nudging and pushing on VL2 was remarkably successful, and the potential scientific yield is high because of the acquisition of samples from newly exposed surfaces that were shielded from ultraviolet radiation and aeolian deposition. The behavior of rocks during nudg-

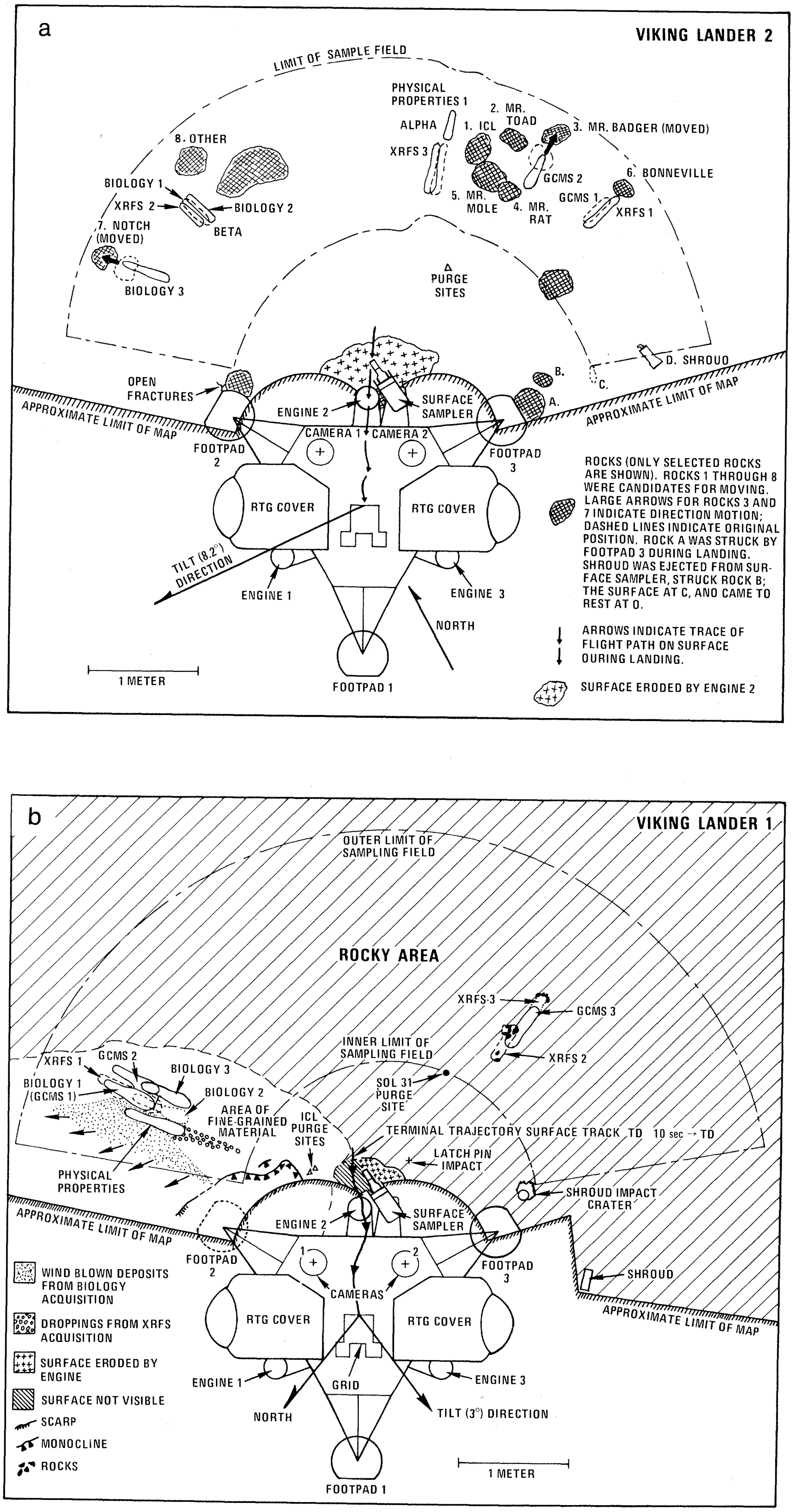

Fig. 2. (a) Plan view of VL2 showing the spacecraft and its orientation, locations of sample sites, locations of selected rocks [rocks 2, 3, 4, and 5 were named from characters in the book *Wind in the Willows* (*13*); rock 6 was so named because of its shape; rock 8 was simply named (Other rock); the rock 1 name stands for Initial Computer Load (*14*)], and surface disturbances relevant to the physical properties experiment; RTG, radioisotope thermal generator; acquisition, rock push, and purge times are summarized in Table 2. (b) Plan view of VL1, showing activities through sol 91; TD, touchdown.

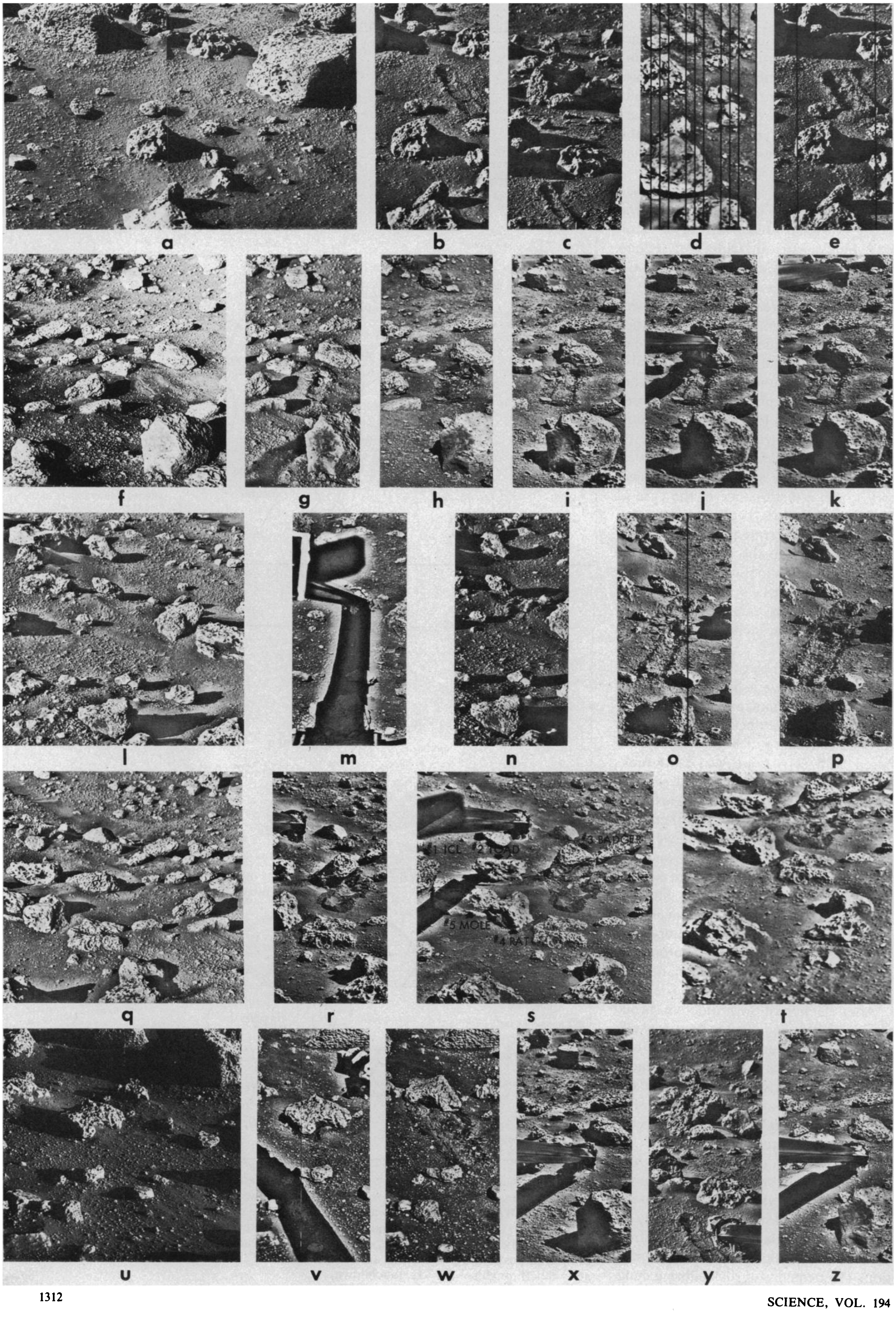
#1 ICL
#2 TOAD
#3 BADGER
#5 MOLE
#4 RAT
a
b
c
d
e
f
g
h
i
j
k
l
m
n
o
p
q
r
s
t
u
v
w
x
y
z

ing and pushing varied. Rock 1 (ICL) did not move, perhaps because it is deeply buried. Rock 3 (Mr. Badger) moved in a complicated way. During the first push (sol 34), Mr. Badger probably tilted up, rotated counterclockwise (as viewed in Fig. 2), and translated about 10 cm (Fig. 3r). A picture taken just prior to that in Fig. 3r shows that the collector head was trapped and leaned upon by Mr. Badger, driving the collector head to the right. The second push was accompanied by tilting and skidding as shown by the smooth-appearing skid marks in Fig. 3s. Rock 7 (Notch) plowed and furrowed while rotating clockwise (Fig. 3n). Rock 6 (Bonneville) merely tipped backward away from the lander (Fig. 3j). None of the rocks noticeably spalled or chipped while being nudged and pushed; these results suggest that a thick weathered rind is not present on them. Thus, the surface materials may be a mixture of weathered products and unweathered rocks.

On sols 46, 47, 57, and 58 the prime goal was to deliver "rocks" from the Beta and Alpha sites (Fig. 2a) to the x-ray fluorescence experiment (XRFS). No sample was found to be present in the XRFS chamber. The same result obtained when the sol 8 "coarse fraction" from the biology acquisition was purged into the XRFS funnel on sol 13. Examination of the purge site after the sol 28 biology acquisition also gave no evidence for purged coarse material. Thus, it appears that the smaller lumps in Fig. 3, a and l, are chiefly from weakly cohesive clods of materials with grains finer than 2.0 mm etched out by weathering and wind. Rocks are present, however, because one about 2.7 cm in diameter was purged along with finer ones after the sol 31 (GCMS) acquisition from the Bonneville site (Fig. 4b), and finer ones < 2.0 mm) were purged after the sols 29 and 30 XRFS acquisition (Fig. 4c).

Small, thin, platy objects suggesting a surface crust are ubiquitous. They are particularly evident at the Bonneville site (Fig. 3, f, g, and h) where they have been domed by trenching (Fig. 3g), have slid along the surface by the backhoe during retraction (Fig. 3h), and have churned up (Fig. 3, j and k). Some have been exposed by engine exhaust erosion (Fig. 1) and other trenching operations (Fig. 3c, backhoe pile). These objects may be chiefly fractured, weakly cohesive, platy, soil clods, but others may be rocks because larger rectangular rocks with planar surfaces occur elsewhere in the sample field.

Martian soil properties. A variety of martian soils have been accessible to VL1 and VL2, and a number of essentially qualitative tests have been carried out to assess their properties. A number of objects, including spacecraft components and fragments of martian rock,

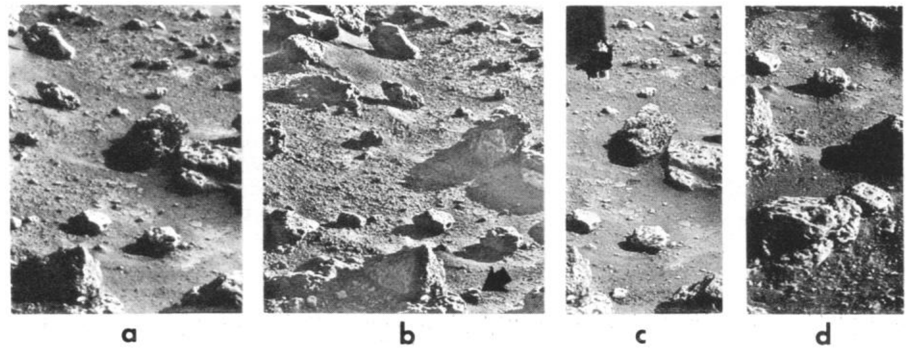

Fig. 4. Purge sites from VL2. (a) The site before any material was purged on to the surface (event L.L.T. 001 092856 Fr 22 A007/001; sun from right; SEA, 47.7°). The site is located between the two large rocks at the bottom of the picture. (b) The purged material (coarse fraction) from the GCMS sample (GCMS-1) obtained on sol 21 (event L.L.T. 023 070941 Fr 22 A178/023; sun from right; SEA, 24.2°). Note the rock (2 to 3 cm) which was purged (arrow). (c) the purge site after the collection of the first biology sample (Beta site) may show several millimeter-sized particles. The fines were delivered to the instrument and the coarse particles purged (event L.L.T. 030 113747 Fr 22A251/030; sun from right; SEA, 59.2°). (d) Physical properties purge site from the Alpha acquisition (PP1) (event L.L.T. 057 093259 Fr 106 C044/057; sun from right; SEA, 18.3°).

Fig. 3. Sample sites from VL2 (all L.L.T. times refer to the time of start of the picture scan). (a) Beta site before acquisition [event L.L.T. 006 (sol) 173000 (hours, minutes, seconds) Fr 21 (lander number, camera number) A044/006 (picture number/sol); sun from left; SEA (sun elevation angle), 25.0°]. (b) Beta site after acquisition (*15*) for the first biology (Biology-1) experiment on sol 8 (event L.L.T. 015 165959 Fr 21 A110/015; sun from left; SEA, 28.9°). (c) Beta site after acquisition for the second biology sample (Biology-2) on sol 28 (event L.L.T. 028 180459 Fr 21 A230/028; sun from left; SEA, 16.8°). (d) Beta site after acquisition for the XRFS experiment (XRFS-2) on sol 46 (event L.L.T. 047 114550 Fr 21 B141/047; sun from right; SEA, 57.0°). The black lines were introduced in the analog-to-digital conversion on Earth and will be corrected in later versions. The "fuzzy" appearance of the picture is due to the use of the red-sensitive diode. (e) Beta site after acquisition of the second part of the XRFS sample (XRFS-2) on sol 47 (event L.L.T. 050 173000 Fr 21 B195/050; sun from left; SEA, 19.4°). (f) Bonneville site before acquisition. The site is the "crack" a little to the right of the center of the picture (event L.L.T. 000 172959 Fr 22 A005/000; sun from left; SEA, 25.6°). (g) Bonneville site after first acquisition for the organic chemistry experiment (GCMS-1) on sol 21 (event L.L.T. 021 173959 Fr 22 A162/021; sun to left; SEA, 21.7°). (h) Bonneville site after first acquisition on sol 29 for the XRFS experiment (XRFS-1) (event L.L.T. 029 141959 Fr 22 A 242/029; sun from right; SEA, 57.5°). (i) Bonneville site after second part of first acquisition for XRFS on sol 30 (XRFS-1) (event L.L.T. 030 111810 Fr 22 A247/030; sun from right; SEA, 58.1°). (j) Bonneville rock during the nudge sequence with the collector head of the surface sampler in contact with the rock on sol 45 (event L.L.T. 045 101139 Fr 22 B116/045; sun from right; SEA, 49.6°). (k) Bonneville rock after retraction of the surface sampler boom on sol 45. The rock fell back almost in the same location (event L.L.T. 045 101454 Fr 22 B117/045; sun from right; SEA, 50.0°). (l) Alpha site before acquisition (event L.L.T. 000 172959 Fr 22 A005/000; sun from left; SEA, 25.6°). (m) Alpha site with collector head in surface during physical properties sequence (event L.L.T. 056 142945 Fr 22 C023/056; sun from left; SEA, 45.9°). (n) Physical properties trench at the Alpha site after removal of the collector head (event L.L.T. 056 172759 21 C031/056; sun from left; SEA, 18.3°). (o) Third XRFS acquisition trench (XRFS-3) at Alpha site after first pass (event L.L.T. 057 094059 22 C045/057; sun from right; SEA, 44.2°). (p) Second part of third XRFS acquisition (XRFS-3′) at the Alpha site (event L.L.T. 058 093900 22 C053/058; sun from right; SEA, 43.8°). (q) Mr. Badger (rock 3) site before rock push and sample acquisition from a newly exposed surface under the rock (event L.L.T. 000 172959 Fr 22 A005/000; sun from left; SEA, 25.6°). This picture is a continuation of (l) above. (r) Mr. Badger after first push on sol 34 (event L.L.T. 034 104810 Fr 22 B030/034; sun from right; SEA,55.0°). (s) Mr. Badger after second push exposing its bottom (event L.L.T. 037 122436 Fr 22 B047/037; sun from right; SEA, 59.0°). (t) Acquisition site for the second GCMS sample (GCMS-2) from under the newly exposed surface of rock 3 on sol 37 (event L.L.T. 044 115841 Fr 22 B115/044; sun from right; SEA, 57.8°). The use of the red-sensitive diode accounts for the fuzzy picture. (u) Notch rock (rock 7) before acquisition for biology on sol 51 (Biology-3) under the rock (event L.L.T. 036 070059 Fr 21 B040/036; sun from right; SEA, 21.7°). (v) Notch rock after a "nudge" on sol 45 to determine if the rock is movable (event L.L.T. 045 103259 Fr 21 B121/045; sun from right; SEA, 52.1°). (w) Notch rock after a "push" and sample acquisition on sol 51 for biology (Biology-3) (event L.L.T. 051 102459 Fr 21 B204/051; sun from right; SEA, 50.4°). (x) Backhoe after penetrating surface at Bonneville (event L.L.T. 021 101058 Fr 22 A 154/021; sun from right; SEA, 52.2°). (y) Backhoe after penetrating surface at the Beta site (event L.L.T. 028/16113 Fr 21 A227/028; sun from left; SEA, 35.3°). (z) Backhoe after penetrating into the GCMS-1 trench rim at Bonneville (event L.L.T. 029 134038 Fr 22 A239/029; sun from right; SEA, 55.9°).

have also impacted the surface, permitting interpretations of some soil properties from the surface deformations developed. In general, a consistent picture has emerged.

Fortunately, VL1 arrived in a location where one of its footpads rested on a relatively dense, rocky soil, and another on a relatively loose granular deposit. Both visible VL2 footpads rest on a rocky soil similar to that under at least one of the VL1 footpads. Of the soils encountered, the most interesting from a physical point of view is the loose material at the VL1 site.

This soil has been penetrated to a depth greater than 16 cm by footpad 2, and, in fact, it is possible that the footpad has gone completely through a fairly thin coating of the soil and rests on a harder underlying surface. The soil has apparently flowed around the footpad after the impact and completely hides it from view. On Earth this behavior is consistent with that of fine-grained soils in a relatively very loose condition with porosities greater than approximately 60 percent and densities of about 1 g/cm^3. However, if the footpad came to rest in the soil which it penetrated, the penetration by footpad 2 is also consistent with a weakly cohesive, fine-grained material with a bulk density between 1.4 and 1.6 g/cm^3 (*2*). Further tests on Mars will be required to distinguish between the low-density (1 g/cm^3) and high-density (1.5 g/cm^3) models. Tests in a terrestrial laboratory (*5*) appear to indicate that the presence of air in soil pores contributes to the flow phenomenon. It is not clear what part the martian atmosphere played in the footpad impact, but, if the presence of an atmosphere was important, this loose martian soil may be even more porous than the above figures, based on Earth tests, suggest. The weakness and porosity of the soil are confirmed by the presence of numerous pits caused, in the vicinity of VL1, by rock fragments and soil clods ejected by the interaction of the descent engine exhaust with the martian surface.

The same soft soil material was also tested by the surface sampler in the course of obtaining material for the scientific instruments. The nature of the sampler's interaction with the surface suggests a varying but thin (a few centimeters thick) soil cover over a harder substratum. The record of motor currents, as an indication of soil resistance forces during sampler-soil interaction, is inconclusive. The motor currents have generally been small, but they may also have developed by contact of the sampling head with the hard underlying layer

Table 2. Surface sampler activities related to the physical properties investigation on VL2. Listed local lander times (L.L.T.) correspond to: (i) time of the extension command for shroud ejection; (ii) time of the command for the collector head to open just before extension; (iii) time of the extension command for nudges and pushes; and (iv) time of the vibration command for purges. Positions from the surface sampler potentiometer readouts are as follows: azimuths measured from a line 80° counterclockwise from the $(+)Y_L$ direction (direction from camera 2 to camera 1). Azimuths should be reduced by 0.3° because of boom override due to lander tilt; extensions are reported here in inches (1 inch = 2.54 cm) to be consistent with engineering units used for the surface sampler systems and represent the increase in the length of the boom from the stowed position; elevations are measured from the Z-Y plane (plane parallel to the upper surface of the lander body) passing through the surface sampler elevation axis; (+) is angle below plane, (−) angle above plane; N.A., not applicable.

Item	Activity	L.L.T.				Surface sampler positions		
		Sol	Hour	Minutes	Seconds	Azimuth (deg)	Extension (inches)	Elevation (deg)
a	Shroud ejection (see Fig. 2a)	01	10	52	41	255.4	10.2	38.9
b	Biology-1, sample (Beta, see Fig. 3b)	08	16	10	20	124.7	85.2 91.7 79.6	23.1
c	GCMS-1, sample (Bonneville, see Fig. 3, g and h)	21	10	10	19	216.3	93.6 88.8 97.3 91.2	30.0
d	Purge (GCMS-1) (see Fig. 4b)	21	10	53	46	190.4	39.9	36.3
e	Biology-2, sample (Beta, see Fig. 3c)	28	16	10	31	126.0	85.2 91.7 79.6	23.1
f	Purge (Biology-2)	28	17	44	46	190.4	39.9	36.3
g	XRFS-1, sample (Bonneville, see Fig. 3, h and i)	29	13	39	56	217.5	93.0 99.4 90.9	29.4
		30	10	39	56	217.5	93.0 99.4 90.9	30.0
h	Purge (XRFS-1) (see Fig. 4c)	29	14	05	45	190.4	39.9	36.3
		30	11	05	45	190.4	39.9	36.3
i	Rock 1 nudge (ICL, see Fig. 3m)	30	11	29	34	186.4	75.4 78.6	33.2 30.6
j	Rock 3 push (Mr. Badger, see Fig. 3r)	34	10	39	40	201.1	84.4 96.5 82.0	30.6 30.0
k	Rock 3 push (Mr. Badger, see Fig. 3s)	37	10	06	55	200.5	81.1 101.2 82.0	29.4, 28.1
l	GCMS-2, sample (under Mr. Badger, see Fig. 3t)	37	16	14	48	201.1	93.0 84.1 87.0 93.6	28.8 20.5, 30.0
		37	16	51	50	201.1	93.0 84.1 87.0 93.6	29.4 20.5, 30.6
m	Purge (GCMS-2)	40	16	01	01	192.9	39.9	36.3
n	Rock 6 nudge (Bonneville, see Fig. 3, j and k)	45	10	10	28	217.5	99.1 103.0 98.0	25.6, 26.2
o	Rock 7 nudge (Notch, see Fig. 3v)	45	10	22	07	105.8	84.1 87.1 60.2	23.1, 22.4
p	XRFS-2, sample (Beta, see Fig. 3, d and e)	46	13	07	52	123.5	85.2 91.7 83.1	23.1
		46	13	47	52	123.5	85.2 91.7 83.1	23.7
		47	13	07	52	123.5	85.2 91.7 83.1	23.7
		47	13	47	52	123.5	85.2 91.7 83.1	23.7

Table 2 continued

Item	Activity	L.L.T.				Surface sampler positions		
		Sol	Hour, minutes, seconds			Azimuth (deg)	Extension (inches)	Elevation (deg)
q	Purge (XRFS-2)	46	13	16	34	123.5	83.1 40.2	−11.0
		46	13	56	34	123.5	83.1 40.2	−11.0
		47	13	16	34	123.5	83.1 40.2	−11.0
		47	13	56	34	123.5	83.1 40.2	11.0
r	Rock 7 push (Notch, see Fig. 3w)	51	06	22	49	106.4	86.7 98.0 60.2	21.8, 21.8
s	Biology-3, sample (under Notch, see Fig. 3w)	51	06	55	35	107.1	93.6 78.1 88.0 94.6 82.0	20.5 15.5, 21.8
t	Purge (Biology-3)	51	09	03	49	190.4	43.9	36.3
u	Physical Properties-1, sample, temperatures (Alpha, see Fig. 3m)	56	14 14	15 33	58 12	180.9	88.0 95.2 88.0	28.8
v	Physical properties magnification mirror image of front porch and footpad 2 (picture via mirror 1)	56	14 14 15 15	41 58 01 03	58 44 18 48	8.5 120.9 120.9 118.4	18.6 18.6 18.6 18.6	0.3 28.1 33.2 33.2
w	Physical properties retro-engine 2 (pictures via boom mirror 2)	57	06 06 06	49 52 54	37 4 31	255.4 251.6 247.8	N.A. N.A. N.A.	40.1 40.1 40.1
x	Purge (Physical Properties-1) (see Fig. 4d), coarse particles	57	07	00	16	192.3	39.9	36.3
y	XRFS-3, sample (Alpha, see Fig. 3, n and o)	57	08	08	29	180.3	75.2 81.7 63.3	33.2
		57	08	53	29	180.3	75.2 81.7 63.3	33.2
		58	08	08	29	179.0	75.2 81.7 63.3	32.5
		58	08	53	29	179.0	75.2 81.7 63.3	32.5
z	Purges (XRFS-3)	57	08	12	40	180.3	64.4	−18.0
		57	08	57	40	180.3	64.4	−18.0
		58	08	12	40	179.0	64.4	−18.0
		58	08	57	40	179.0	64.4	−18.0

Items: (a) Shroud ejected at 3.2 m/sec, struck a rock near footpad 3 at 3.7 m/sec, ricocheted from the rock, impacted the surface 0.6 m beyond the rock, and came to rest 1.1 m beyond the rock; the rock near footpad 3 moved a small amount as a result of the impact. (b) Trenched by extending after surface contact and then retracting; trench about 40 cm long from rim to rim, 7.6 cm wide from rim to rim; coarse fraction purged to the XRFS funnel but no sample was received; small lumps in and around the trench are probably chiefly clods. (c) Trenched by retracting after surface contact, then extending followed by retracting; trench about 25 cm long, 5.6 cm wide at the far tip, 7.3 cm wide at the near tip; the collector head tunneled beneath the crust doming surface, crust near the far tip. Platy fragment of crust about 7 cm in diameter and 1 cm thick was moved by the backhoe. (d) Purged material larger than 2.0 mm; fragment 2.7 cm in diameter and additional finer grains or clods 2 mm and larger. (e) Trenched by extending after surface contact and then retracting. Trench about 40 cm long, 7.6 cm wide. (f) Purged material should be larger than 2.0 mm; no evidence for purged coarse particles. (g) Trenched by extending after surface contact and then retracting; first acquisition extension lifted a rock at the far end of the trench about 0.4 cm; large platy fragments of crust in and around the trench and fine-grained material in debris pile at the tip (Fig. 3h); the trench in Fig. 3i is 28 cm long, 7.7 cm wide at the far end, 9.4 cm wide at the near end; material at the far end has spread laterally to the trench azimuth because of rock; rectangular fragment about 3 cm on an edge and 1 cm thick. (h) Purged material larger than 2.0 mm; a large fragment has been displaced and purged; material 5 mm and smaller has been added. (i) Nudged by elevating after surface contact, then extending, and then retracting; commanded extension was 83.1 inches; the rock did not move. (j) Pushed by elevating after surface contact, then extending, and then retracting; the rock was pushed about 10 cm away from the lander; rotated about 60° or 70° counterclockwise about vertical axis, and tilted about 45° about a horizontal axis; the collector head went beneath the rock which leaned on the collector head, deflecting it to the right, and forced the excavation of a trench in front of the rock. (k) Pushed by elevating after surface contact, then extending, and then retracting; the rock was pushed an additional 12 or 13 cm away from the lander with little rotation; commanded extensions compared with measurements of the rock indicate that the rock tilted backward and then forward to its present position. (l) Trenched by retraction after contact with the surface to clear debris away; then elevating, extending and deelevating to touchdown; then extending for sample acquisition, and then retracting; trench about 30 cm long, 10 cm wide; sample was delivered to GCMS from the first acquisition although the surface sampler made two acquisitions. (m) Purged material should be larger than 2.0 mm; no evidence for purged material. (n) Nudged by elevating after surface contact and then extending; reversal of elevations related to boom sag and overtravel; the rock rotated about a nearly horizontal axis, and points on the front surface of the rock were displaced upward about 1 cm during nudge (Fig. 3j); the rock fell back again after the retraction of the collector head, pushing materials from the trench rim into the trench (Fig. 3k). (o) Nudged by elevating after surface contact and then extending; the rock rotated in a horizontal plane about an axis on the right side of the rock; the left edge of the rock was displaced about 3.8 cm. (p) Final trench about 30 cm long, 8 cm wide; sampled to collect rocks but little or no sample was received; some fragments at the surface may be rocks, but most are clods of soil (see also items b and f). (q) Purged material smaller than 2.0 mm; no evidence for purged material at the trench site. (r) Pushed by elevating after surface contact, and then extending; rock rotated about 50° counterclockwise in a horizontal plane; translated about 24 cm from the original position by sliding away from the gimbal axis of the surface sampler (Fig. 3v). (s) Trenched by retracting to clear away possible contaminating debris; then elevating, extending, and deelevating to surface contact; then extending for sample acquisition followed by retracting; backhoe trench about 7.6 cm wide; extension trench difficult to measure (trench length about 46 cm). (t) Purged material larger than 2.0 mm; some purged material, generally small grains (≤ 2.0 mm). (u) Trenched by extending after surface contact and then retracting; trench about 28 cm long and 6 cm wide near the tip; the trench is very shallow, probably because of interference by excavated rock which is about 3 by 6 cm. (v) A picture of the front porch to study soil with magnification mirror; a series of three pictures to determine the conditions of the footpad 2 temperature sensor and material around the footpad not viewable directly. (w) A series of three pictures to study retro-engine erosion at touchdown. (x) A few objects, 0.5 cm and smaller, were purged from the collector head. (y) Trenched by extending after surface contact and then retracting; the sol 57 trench is 56 cm long, 7.3 cm wide; the largest clods are 4.0 cm in diameter; deformation producing clods extends 7.0 cm from the rim in lateral directions; the sol 58 trench is the same size as the sol 57 trench but overlaps it and extends the lateral deformation only a small amount to the left. (z) Material purged smaller than 2.0 mm.

rather than by soil interaction. The appearance of the sample trenches and trench walls is consistent with that of an excavation in a weakly cohesive (10^3 to 10^4 dyne/cm^2) fine-grained material. Some of the material behavior deduced from the performance of the XRFS experiment is also consistent with this conclusion (6).

Generally, all mineral particles experience surface interaction forces on contact with each other. With larger particles (larger than 100 μm) these surface forces are unimportant in comparison with the bulk forces arising from the mass of the particle in the gravitational field. Consequently, deposits of such large particles tend to exhibit fairly dense packing arrangements (porosities less than 50 percent) as the particles roll or slide over one another under gravitational forces. With smaller particles, the surface forces are more important

Table 3. Current best estimate of soil properties deduced from VL1 and VL2 data. Particles as used here include clods as well as individual mineral and rock grains; thus the estimates of particle sizes must be considered approximate and preliminary. The frequency of rocks 10 cm and larger at the VL2 site is twice as large as that at the VL1 site (*8*). The estimated density of materials after delivery to the XRFS experiment is 1.1 ± 0.15 g/cm^3 (*6*).

Property	Viking 1		Viking 2
	Sandy Flats	Rocky Flats	Bonneville and Beta
Bulk density (g/cm^3)	1 to 1.6	1.8	1.5 to 1.8
Particle size (surface and near surface)			
10 to 100 μm (%)	60	30	30
100 to 2000 μm (%)	10	30	30
Angle of internal friction	20° to 30°	40° to 45°	40° to 45°
Penetration resistance (dyne cm^{-2} cm^{-1})	3×10^4	6×10^5	6×10^5
Cohesion (dyne/cm^2)		10^3 to 10^4	10^4
Adhesion (dyne/cm^2)		10^1 to 10^2	
Coefficient of sliding friction		0.55 to 0.65	

and particles coming in contact with one another tend to stick at the contact points. The degree to which they adhere depends on the contact forces, whose strength in turn depends on the cleanliness of the particles. Forces due to van der Waals and electrostatic interactions as well as surface tension in the case of grains surrounded by thin films of physically bound liquid water all play a part on Earth; the relative contributions of these forces are not known on Mars. The amount of water (approximately 1 percent by weight) recognized by the GCMS experiment (*7*), if in liquid form, could cause some cohesion in a fine soil, although the film thickness is probably not great enough to give rise to meniscus forces. In consequence, the properties of the fine-grained material adjacent to VL1 are consistent with those of a loose fine soil probably drifted into place by the martian wind. After deposition, depending on time and the processes at work, cementation of the particles could also occur.

Around and between the rocks and rock fragments visible near both spacecraft are other soil areas. The material in these areas seems to be denser and stronger than the soil discussed above, but, on the basis of the evidence of the sampling tests, it exhibits no unusual strength or density. There appear to be visual indications, at least in some areas, that this soil may be somewhat cohesive, or possibly cemented. This has given rise to speculation that it is a "crust" of granular material cemented with some agent (the word "caliche" has frequently been used). Although this may be possible, the idea does not get strong backing from the results of all the sampling operations. In a test in which the sampler backhoe was brought down in such a possible crust area, the contact switch stopped the sampler when the backhoe had penetrated 1 cm into the crust (Fig. 3, x, y, and z). The force required to cause this penetration is not great, about 10 newtons, and the penetration is about the same as the sampler achieves in a medium-dense, fine-grained, normal terrestrial soil ("lunar nominal," for example). The appearance of plates or platy lumps in the material disturbed by sampling is also common in the case of tests on homogeneous, slightly cohesive or slightly cemented normal terrestrial soils.

A summary of the soil properties from VL1 and VL2 is given in Table 3. In spite of the similarities in the soil properties at both sites, there are important differ-

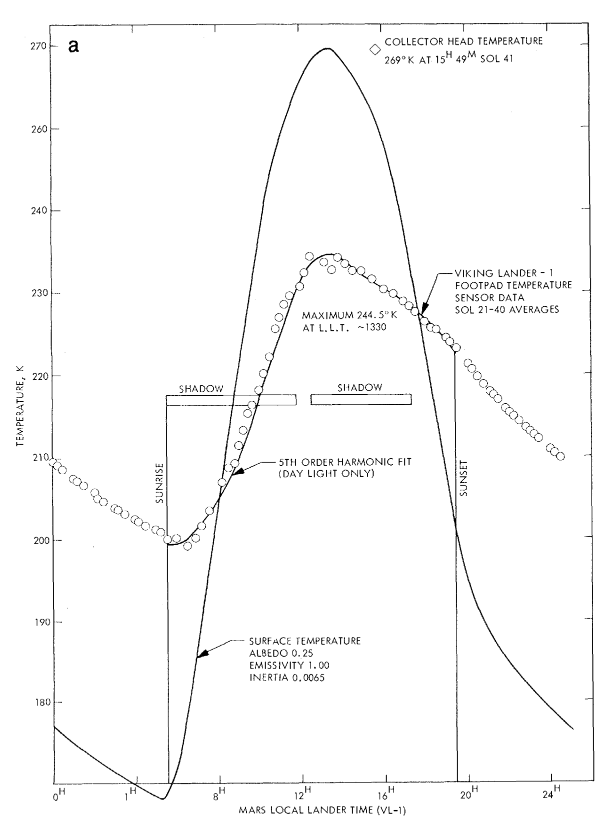

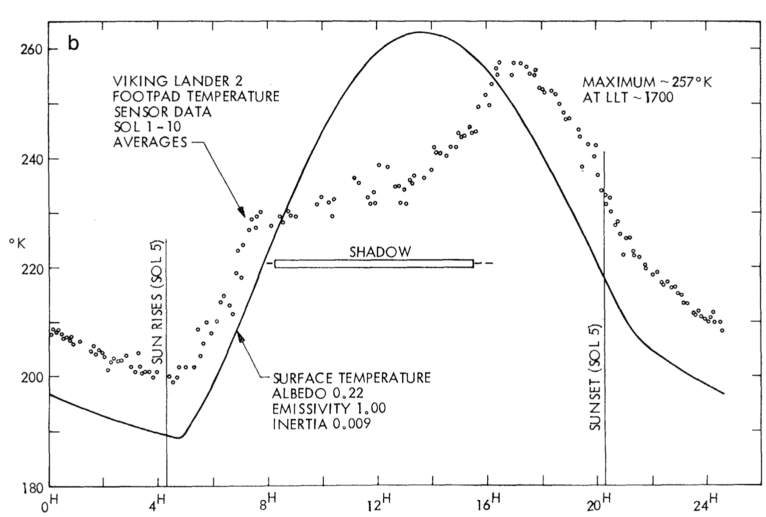

Fig. 5. Footpad 2 temperature sensor plots. Data are obtained only when certain engineering information is requested, and so there are often gaps in the record. Each open circle is an average of from one to ten readings: (a) VL1 temperatures averaged over sol 21 through sol 40 for each 6-minute interval. The fifth-order harmonic fit (*16*) was obtained for daylight hours. The bars marked "shadow" indicate the time when the footpad sensor was in the shadow. The other curve shows the predicted surface temperatures (*17*). The one point at 153000 L.L.T. was obtained by the collector head after being in the soil for 10 minutes. (b) The VL2 temperatures averaged over sol 1 through sol 10 for each 6-minute interval. The bar marked "shadow" indicates the time when the temperature sensor was in the shadow of the lander and supported struts. The solid curve is the predicted surface temperature (*17*). The shift in the time for the footpad temperature maximum is caused by shadowing of the sensor.

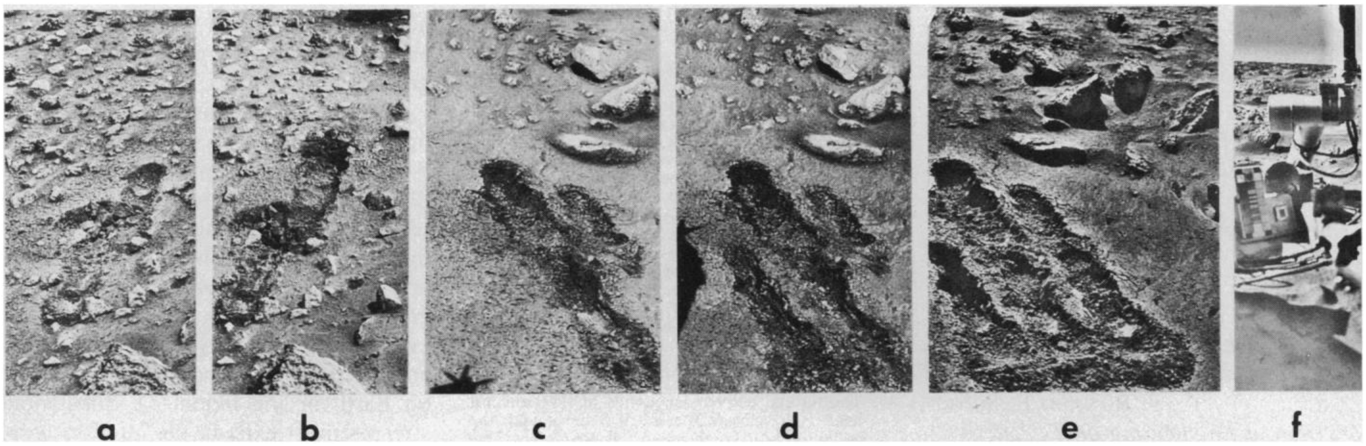

Fig. 6. Lander camera pictures of surface sampler activities on VL1 subsequent to sol 36. (a) Rocky Flats before acquisition of XRFS-3 (event L.L.T. 034 125500 Fr 12 B030/034; sun from right; SEA, 81.6°). (b) Rocky Flats after XRFS acquisition on sol 40 (XRFS-3); two passes or digs were carried out at this site (event L.L.T. 053 140159 Fr 12 B138/053; sun from right; SEA, 65.8°). (c) Sandy Flats before acquisition of PP-1 (event L.L.T. 036 14141 Fr 11 B 058/036; sun from right; SEA, 63.7°). (d) Sandy Flats after physical properties acquisition on sol 41 (PP-1) (event L.L.T. 079 Fr 11 B169/079; sun from right; SEA, 49.2°). The shadow on the left margin is the meteorology boom. (e) Sandy Flats acquisition trench (lower half or right hand trench) for the biology experiment on sol 91 (event L.L.T. 091 090459 Fr 11 B180/091; sun at right; SEA, 47.2°). (f) Top of VL1 after purge of fines on sol 41 (event L.L.T. 041 16009 Fr 12 B107/041; sun from left; SEA, 38.7°). The reference test chart is located in the middle of the picture to the left. The magnification mirror is located just above the center of the picture. The back of the backhoe (which contains two magnets) and the front of the backhoe (in the magnification mirror) can be seen (*18*).

ences. The frequency of occurrence of rocks 10 cm and larger is twice as high at the VL2 site as at the VL1 site, drifts and dunes are absent near VL2, and more vesicular rocks are present at the VL2 site than at the VL1 site (*8*).

Surface temperature measurements. The VL2 parachute phase (*9*) footpad 2 temperature sensor (*1*) survived the shock of touchdown. A complicated insolation function for this temperature sensor on both landers prevents an immediate analysis of the data. Figure 5, a and b, shows temperature plots for both VL1 and VL2. Shadows from the main leg support and secondary supports cause significant deviations from the expected behavior. An attempt was made to image the footpad sensor on VL1, but, because of an improper boom position, the posts where the thermocouples were mounted was missed so that it is not yet known if the sensor is buried or partially covered with surface material. This footpad is buried to a depth of about 16 cm (*2*). In the case of VL2, footpad 2 is not buried and penetrated only 2.5 cm so that it is unlikely that this sensor is in contact with the surface. Pictures will be obtained of the footpad temperature sensors via the boom-mounted mirror.

In addition to the footpad temperature sensor, there is a thermocouple on the bottom of the collector head intended to show that a soil sample did not reach a temperature more than 20°K above the maximum expected surface temperature. Each time the surface sampler boom or collector head moved, a reading was obtained. In particular, upon the command to close the collector head, temperature readings were taken 2 and 4 seconds later. Since the time constant of the thermocouple was found to be of the order of 10 minutes (*10*), most readings are in doubt. An experiment was conducted in which the collector head was left in the surface for 10 minutes. The point is plotted in Fig. 5a. Because the thermocouple is physically bonded to the bottom of the collector head, conduction effects are significant.

Activities on VL1 since sol 36. The third acquisition for the XRFS experiment was obtained on sol 40 from the Rocky Flats site. The coarse fraction was delivered. Subsequent analysis of the sample, based on the chemical composition (a bulk density), indicates that the materials delivered were primarily clods and not rocks (*6*). Figure 6a shows the Rocky Flats site before acquisition of the XRFS sample and Fig. 6b after acquisition on sol 40; two passes or digs were carried out. At the far end of the trench a pile of rocks or clods was left after the acquisition.

The right wall of the physical properties trench (left in Fig. 6d) slid back toward the trench a small amount when the collector head was retracted. This is partly evidenced by the fact that the trench is not as wide as expected. Material on the front porch of the collector head was imaged by the magnification mirror (just to the right of the reference test chart in Fig. 6f). The picture was, however, out of focus so that improved resolution was not realized. After a picture of the backhoe magnets was obtained, the collector head was rotated and vibrated, depositing the fine fraction from Sandy Flats on top of the lander as shown in Fig. 6f. The fines formed a pile and "washed" over the grid, almost completely covering it. Subsequent pictures show that this fine-grained material has moved, presumably by the winds which have been reported to be as high as 15 m/sec (*11*).

The biology team acquired a third sample on sol 91 at Sandy Flats (Fig. 6e). A sample full signal was received, indicating a successful delivery. However, on the way to biology delivery, a partial sample was inadvertently delivered to the XRFS funnel. A subsequent examination of the surface sampler data verified that the delivery sequence to the biology funnel was as planned and had not included those boom movements necessary to deliver to the XRFS funnel as well. It is now believed that, when the collector head was rotated while positioned over the biology funnel, the backhoe suddenly released from a stowed position and propelled trapped surface material into the XRFS funnel. Data received by the inorganic chemistry team (*12*) indicated that ~ 20 cm³ of surface material was now in their sample cell which previously had been empty. The backhoe explanation, however, seems inadequate to explain this large volume. No further surface sampler activities will be attempted on either VL1 or VL2 until after sol 171 (11 January 1977). It is expected that during the Viking extended mission (1977) more experiments will be done on VL1 and VL2. The surface properties will be investigated further; the surface sampler will be used to do penetration tests, dig a deep trench, and better determine the particle size distribution.

RICHARD W. SHORTHILL
Geospace Science Laboratory, University of Utah Research Institute, Salt Lake City 84108
HENRY J. MOORE II
U.S. Geological Survey, Menlo Park, California 94025
ROBERT E. HUTTON
Applied Mechanics Laboratory, TRW Systems Group, Redondo Beach, California 90278
RONALD F. SCOTT
Division of Engineering and Applied Science, California Institute of Technology, Pasadena 91125
CARY R. SPITZER
NASA Langley Research Center, Hampton, Virginia 23665

References and Notes

1. R. W. Shorthill, R. E. Hutton, H. J. Moore II, R. F. Scott, C. R. Spitzer, *Science* **193**, 805 (1976).
2. R. W. Shorthill, H. J. Moore II, R. F. Scott, R. E. Hutton, S. Liebes, Jr., C. R. Spitzer, *ibid.* **194**, 91 (1976).
3. "Soil," as used here, refers to the relatively fine-grained, near-surface materials of Mars that have been deformed as a result of the landing of the spacecraft and which have been acquired by the collector head. Large objects (about 2 cm and larger) that obviously have large cohesion are termed rocks, fragments, and blocks. The word "sample" usually indicates that which was analyzed by the three active soil analysis experiments: biology, GCMS, and XRFS. The word "acquisition" usually refers to the process of obtaining soil.
4. "Sol" is defined as a martian day (24.62 hours). Sol 0 for Viking 1 was 20 July 1976, and sol 0 for Viking 2 was 3 September 1976.
5. L. V. Clark, NASA Langley Research Center, letter to I. W. Ramsey, Jr., Viking Project Office, 12 October 1971. Laboratory tests were carried out at the NASA Langley Research Center, Hampton, Virginia. Full-scale footpads were dropped in different soils which had been prepared with various densities and grain sizes. The velocities at impact were in the range of those encountered on Mars.
6. B. C. Clark, A. K. Baird, H. J. Rose, Jr., P. Toulmin III, K. Keil, A. J. Castro, W. C. Kelliher, C. D. Rowe, P. H. Evans, *Science* **194**, 1283 (1976).
7. K. Biemann *et al.*, *ibid.* p. 72.
8. T. A. Mutch *et al.*, *ibid.*, p. 1277.
9. A. O. Nier, W. B. Hanson, A. Seiff, M. B. McElroy, N. W. Spencer, R. J. Duckett, T. C. D. Knight, W. S. Cook, *ibid.* **193**, 786 (1976).
10. Wind tunnel tests were conducted to measure the time constant in the atmosphere. The tests were performed at McDonald Douglas Laboratories, St. Louis, Missouri.
11. S. L. Hess *et al.*, *Science* **194**, 78 (1976).
12. This information was provided by P. Toulmin, team leader of the inorganic chemistry team.
13. K. Grahame, *The Wind in the Willows* (Scribner's, New York, 1961).
14. If commands had not been sent to the lander, then on sol 9 the surface sampler would have attempted to sample at the preprogrammed site, ICL rock (rock 1).
15. The normal delivery sequence of the collector head is to vibrate the lid at 8 hertz with the collector head in the inverted position so that the fines pass through a 2-mm screen. The coarse fraction (≥ 2 mm) left in the collector head is then purged from the collector head if the lid is rotated back 180° and vibrated at 4 hertz. Inside the collector head are a series of teeth placed there to disaggregate clods and weakly cohesive material. The purge is usually done on the surface in view of the cameras.
16. The fifth-order harmonic fit was done by J. Mitchell of the meteorology team. The diurnal harmonic (zero and first-order harmonics) curve has its maximum at 154200 L.L.T.
17. The predicted surface temperature curve was furnished by H. H. Kieffer, team leader of the infrared thermal mapping experiment.
18. R. B. Hargraves, D. W. Collinson, R. E. Arvidson, C. R. Spitzer, *Science* **194**, 1303 (1976).
19. We acknowledge the continuing aid and support given to the physical properties investigation team by the surface sampler team. The lander imaging team kindly furnished the pictures (more than 40) used in this report. We also thank P. Duffy for his assistance as the physical properties intern for the month of September. We thank L. Crafton for typing the manuscript several times and for attending to many administrative matters. We thank Dr. D. W. Collinson for his review of the manuscript and discussions of the physics of the soil properties of Mars. Dr. S. Liebes, Jr., provided the mensuration data for the rock pushes and nudges. We thank Dr. R. Goldstein for his support during sol 0 for VL1 and VL2 and throughout the mission. This work was supported by NASA contract NAS1-12705 to the University of Utah Research Institute, NASA order L-9714 to the U.S. Geological Survey, and NASA contract NAS1-10534 to TRW Systems, Inc.

15 November 1976

The Viking Seismic Experiment

Abstract. *A three-axis short-period seismometer is now operating on Mars in the Utopia Planitia region. The noise background correlates well with wind gusts. Although no quakes have been detected in the first 60 days of observation, it is premature to draw any conclusions about the seismicity of Mars. The instrument is expected to return data for at least 2 years.*

A three-axis short-period seismometer was delivered to the surface of Mars by Viking Lander 2 on 3 September 1976 and began to operate at 00:53:01 G.M.T. on 4 September shortly after noon, lander local time (L.L.T.) (*1*).

An important first step in characterizing the seismology of a planet is to determine the level and nature of the background noise. In the case of Earth, the main sources of background noise are the ocean and the atmosphere. These noises, termed microseisms, were studied extensively in the early days of terrestrial seismology but are no longer of much interest since they are now well understood. This "noise" in the case of a first seismic experiment on Mars actually contains useful micrometeorological information and must be well understood before seismic events can be confidently identified.

The ultimate goals of a seismic experiment on a planet are to determine the level of seismic activity and the internal structure. To achieve these requires a long-lived seismic network. Secondary goals are monitoring meteoroid impacts and establishing the nature of the background noise.

Although Mars has such well-developed tectonic features as fractures, grabens, and youthful-appearing volcanoes, there is no evidence for the kind of plate tectonics that is responsible for most of the seismic activity on Earth. On the other hand, large areas of Mars appear to be grossly out of hydrostatic equilibrium, as evidenced by gravity anomalies which are much more pronounced than those on Earth or the moon (*2*). Substantial stresses must exist in the interior in order to support the nonhydrostatic shape and, in particular, the young volcanic terrains. Although the level of seismic activity on the moon is much less than that on Earth, thousands of small quakes are recorded there each year by the Apollo seismic network. We would therefore expect that seismic events also occur on Mars, although their magnitude and frequency cannot be estimated.

Description of the Viking seismometer. The Viking seismometer package includes sensors, amplifiers, filters, automatic event detectors, data compactors, and temporary data storage. The instrument package, measuring 12 by 15 by 12 cm and weighing 2.2 kg, is located on the top of the lander's equipment bay near the attachment of leg 1. The nominal power consumption is 3.5 watts. The useful frequency range is 0.1 to 10 hertz with a minimum ground amplitude resolution of 2 nm at 3 hertz and 10 nm at 1 hertz. The maximum magnification is 218,000 at 3 hertz when the received signal is plotted at a scale of 0.436 mm per digital unit of seismometer output. The Viking instrument thus has a maximum sensitivity equivalent to that usable at a relatively quiet site on Earth (Fig. 1).

The sensors are three matched, orthogonally mounted (one vertical and two horizontal), inertial velocity transducers. In each sensor a mass-coil assembly is supported on two booms by two elastic hinges (Bendix Free-Flex) in such a way that the flat transducer coil is poised between the facing poles of two channel magnets arranged in series. Motion of the frame causes the transducer coil to move relative to the field of the magnets and generates a signal that is proportional to the relative velocity between the coil and magnets. The undamped natural frequency of each instrument is 4 hertz, the coefficient of damping is 0.6, and the generator constant is 177 volt m^{-1} sec^{-1}.

Each sensor is equipped with a calibration mechanism by which the mass may be magnetically deflected approximately